ACS OMEGA

Open Access

This article is licensed under CC-BY-NC-ND 4.0

http://pubs.acs.org/journal/acsodf

Article

Near-Infrared Ratiometric Hemicyanine Fluorescent Probes for Monitoring Mitochondrial pH Dynamics in Live Cells during Oxidative Stress and Hypoxia

Sushil K. Dwivedi, Dilka Liyana Arachchige, Adenike Mary Olowolagba, Mohamed Mahmoud, Subash Pandey, Tara Vohs, Haiying Liu,* and Rudy L. Luck*

Cite This: *ACS Omega* 2024, 9, 42049−42060

Read Online

ACCESS | Metrics & More | Article Recommendations | Supporting Information

ABSTRACT: Novel near-infrared ratiometric molecules (probes **A** and **B**) produced by linking formyl-functionalized xanthene and methoxybenzene moieties, respectively, onto a xanthene-hemicyanine framework are detailed. Probe **A** exhibited a primary absorption peak at 780 nm and a shoulder peak at 730 nm and exhibited fluorescence at 740 nm↓ (signifies a downward shift in intensity upon acidification) in a pH 9.3 buffer and 780 nm↑ at pH 2.8 under excitation at 700 nm. Probe **B** featured absorptions at 618 and 668 nm at pH 3.2 and at 717 nm at pH 8.6, and fluorescence at 693 nm↑ at pH 3.2 and at 739 nm↓ at pH 8.6, in mostly the red to near-IR region. The ratiometric changes in the intensity of the fluorescent absorptions were reversed between **A** and **B** upon acidification as indicated by the arrows. Theoretical calculations confirmed that there were slight changes in conformation between probes and the protonated molecules, suggesting that the changes in emission spectra were due mostly to conjugation effects. Calculations at the APFD/6-311+g(d,p) level with a solvent described by the polarizable continuum model resulted in pK_a values for **A** at 6.33 and **B** at 6.41, in good agreement with the experimentally determined value of 6.97 and an average of 6.40, respectively. The versatilities of the probes were demonstrated in various experimental contexts, including the effective detection of mitochondrial pH fluctuations. Live cell experiments involving exposure to different pH buffers in the presence of H^+ ionophores, monitoring mitophagy processes during cell starvation, studying hypoxia induced by $CoCl_2$ treatment, and investigating responses to various oxidative stresses are detailed. Our findings highlight the potential of attaching xanthene and methoxybenzaldehyde groups onto xanthene-hemicyanine structures as versatile tools for monitoring pH changes in a variety of cellular environments and processes.

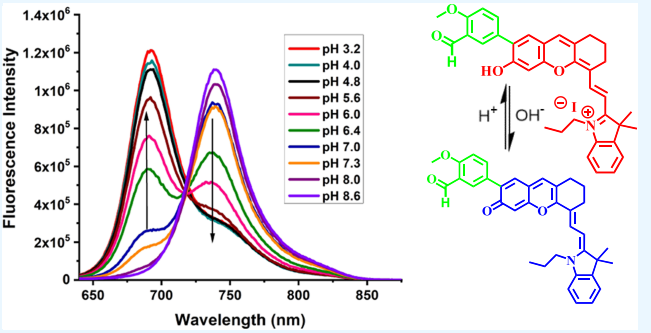

Downloaded via MICHIGAN TECHNOLOGICAL UNIV on January 10, 2025 at 20:30:27 (UTC).
See https://pubs.acs.org/sharingguidelines for options on how to legitimately share published articles.

1. INTRODUCTION

Intracellular pH levels play a very important role in cell proliferation, ion transport, autophagy, endocytosis, apoptosis, and cell polarization. Most organelles have inherent pH buffering capacities to protect compartments from rapid and localized pH changes to maintain cellular activities and functions, such as biological macromolecule degradation in lysosomes,[1−4] post-translational protein modification in the endoplasmic reticulum,[5] processing and sorting of biosynthetic cargo in the Golgi apparatus,[6,7] and energy production in mitochondria.[8,9] Intracellular pH varies significantly within different organelles. It is weakly alkaline in mitochondria (pH ∼ 8.0),[8,9] almost neutral in the cytoplasm, endoplasmic reticulum, cytosol, and nucleus (pH ∼ 7.2), weakly acidic in the Golgi apparatus (pH 6.0−6.7),[10] and acidic in endosomes (pH 5.0−6.3)[11,12] and lysosomes (pH 4.0−5.0).[1−4,13,14] Acidic lysosomes (pH 4.0−5.0) contain a range of hydrolytic enzymes that break down carbohydrates, proteins, nucleic acids, and lipids taken up by endocytosis, phagocytosis, and autophagy.[1−3] Mitochondria are essential for cellular energy production in the form of ATP, storage of Ca^{2+} ions, cellular signaling through reactive oxygen species production, cellular differentiation, proliferation, and apoptosis. Mitochondria require an alkaline matrix at pH 8.0 within the inner membrane for their unique function.[4,8,9] Cells maintain a healthy population of mitochondria by removing dysfunctional ones through a mitophagy process, involving lysosomes to recycle mitochondrial constituents. Abnormal pH leads to cellular dysfunctions and serious diseases, such as glycosylation abnormalities, Golgi fragmentation,[15] lysosomal storage

Received: August 8, 2024
Revised: September 13, 2024
Accepted: September 19, 2024
Published: September 26, 2024

© 2024 The Authors. Published by American Chemical Society

Scheme 1. Structural Reactions of Probes A and B to pH Changes

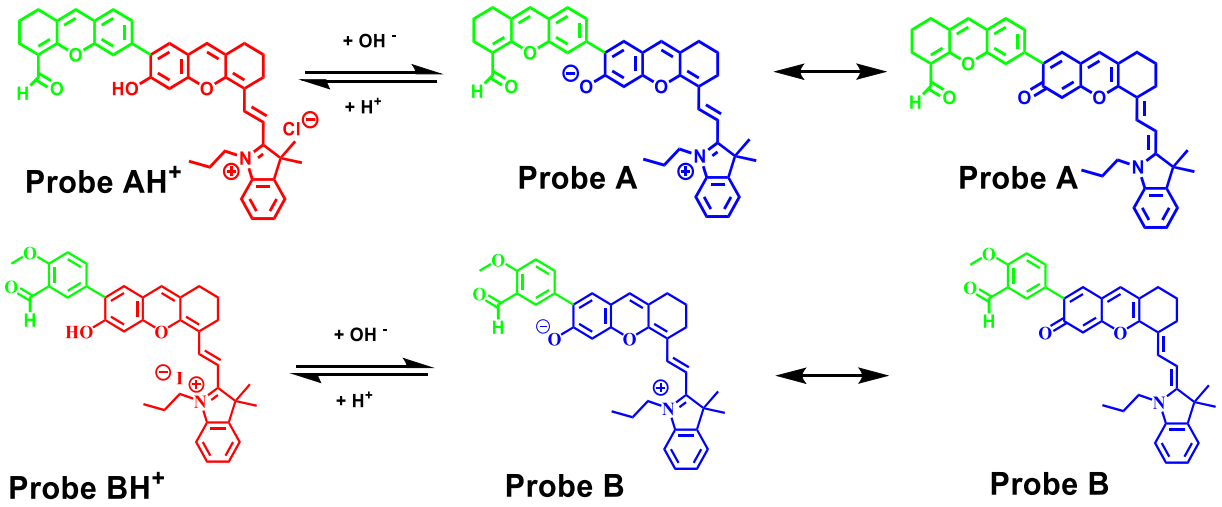

diseases,[16] apoptosis,[17] cancer,[18−20] or Alzheimer's disease.[21,22] Therefore, it is very important to precisely monitor intracellular pH changes in live cells and to track the mitophagy process for an understanding of the physiological and pathological processes involved with cellular functions. Fluorescent probes have become the most powerful tools for monitoring intracellular pH. They possess many remarkable technical and practical advantages over other methods. They can measure the intracellular pH of intact cells and subcellular regions with operational simplicity, high sensitivity, nontoxicity, and excellent spatial and temporal resolution.[9,23−37] Many ratiometric pH fluorescent probes have been developed by incorporating visible fluorophores as donors to near-infrared fluorophores such as rhodamine and cyanine dyes as acceptors in Fluorescence Resonance Energy Transfer (FRET) or through-bond energy transfer configuration to overcome systematic errors of intensity-based fluorescent probes.[38−46] Near-infrared hemicyanine dyes have been an area of focus recently due to their increased penetrating ability compared to UV and visible light. Related structures have been used for in vivo imaging,[41,47] targeting lysosomes,[48] for monitoring cellular mitophagy,[49] and for investigating bone resorption.[50] They also possess near-infrared emission and some feature ratiometric responses to pH changes. Different functional groups such as methoxyl, chloro, bromo, formyl, carboxylic acid, benzyl chloride, tetraphenylethylene, and benzothiazole have been introduced to hemicyanine dyes for the detection of pH changes in live cells.[41]

In this paper, we prepared fluorescent probes (**A** and **B**) by introducing the xanthene and methoxybenzaldehyde moieties respectively to a hemicyanine skeleton to tune fluorescence to longer near-infrared wavelengths and to achieve ratiometric fluorescence responses to pH changes simultaneously (Scheme 1). The probes display ratiometric fluorescence responses based on the deprotonation of the probe's hydroxy group which allows for the formation of the resonance structure with a quinone moiety (Scheme 1).[41,45,51] The results of theoretical calculations affirm this conclusion. The probes show sensitive, reversible, and selective responses to pH changes with good photostability, biocompatibility, and specificity to mitochondria. The probes have been utilized to detect intracellular pH changes in mitochondria triggered by the H^+ ionophore in different pH buffers and to monitor pH fluctuations during mitophagy, under oxidative stresses, and hypoxia.

2. EXPERIMENTAL SECTION

2.1. Instrumentation. A Bruker NMR Spectrometer at 500 MHz (Avance 500) was used to get ^1H and ^{13}C NMR probe spectra. A PerkinElmer Lambda 35 UV/vis spectrometer was employed to collect the probe absorption spectra while a Jobin Yvon Fluoromax-4 spectrofluorometer was utilized to record the probe photoluminescence spectra. Confocal fluorescence cellular imaging experiments were carried out with an Olympus FluoView FV1000 confocal fluorescence microscope (Olympus America Inc.). Cellular Images were gathered and processed with an Olympus FV10-ASW 3.1 viewer, and Photoshop 6.0.

2.2. Reagents. All reagents were obtained from commercial suppliers and used as received without extra purification. The bifunctional 6-bromo-2,3-dihydro-1H-xanthene-4-carbaldehyde scaffold (**3**) was prepared and confirmed according to the reported procedure. The syntheses of the probes are described in Supporting Information.

2.3. General Procedure for Probe Optical and Selectivity Study. DMSO (3.0 mL) was used to prepare the probe stock solution (1.5 mM). All probe optical and selectivity measurements were conducted in 1 cm optical length quartz cuvettes by utilizing 0.1 M citrate−phosphate buffers with 10% DMSO for probe **A** and 30% DMSO for probe **B** for pH ranges from 4.0 to 7.0, and 0.2 M carbonate−bicarbonate buffers in the presence of 10% DMSO for probe **A** and 30% DMSO for probe **B** for pH ranges from 7.0 to 10.3. Solutions of biologically related cationic analytes (Na^+, Sn^{2+}, Fe^{3+}, Zn^{2+}, Mg^{2+}, Ca^{2+}, Cu^{2+}, K^+), anionic analytes (Cl^-, NO_3^-, SO_3^{2-}, IO_3^-, HCO_3^-, SO_4^{2-}, PO_4^{3-}, CO_3^{2-}, GSH), and various amino acids (valine, arginine, glycine, cystine, lysine, tyrosine, serine, and alanine) were prepared in distilled water. Each selectivity measurement was conducted three times with a 50 μM concentration of all possible interferences.

2.4. Cellular Fluorescence Imaging. HeLa cells were matured in Dulbecco's Modified Eagle's Medium with a high glucose concentration of 1 g per liter, augmented with 10% fetal bovine serum (FBS) in a 5% CO_2 and 95% air atmosphere at 37 °C.[38−40,43,44,52−60] Before cellular imaging was conducted, the cells were nurtured with 10 μM probe **A** in

https://doi.org/10.1021/acsomega.4c07303
ACS Omega 2024, 9, 42049−42060

Scheme 2. Detailed Synthetic Approach to Prepare the Probes Based on Xanthene-Incorporated Hemicyanine Dye

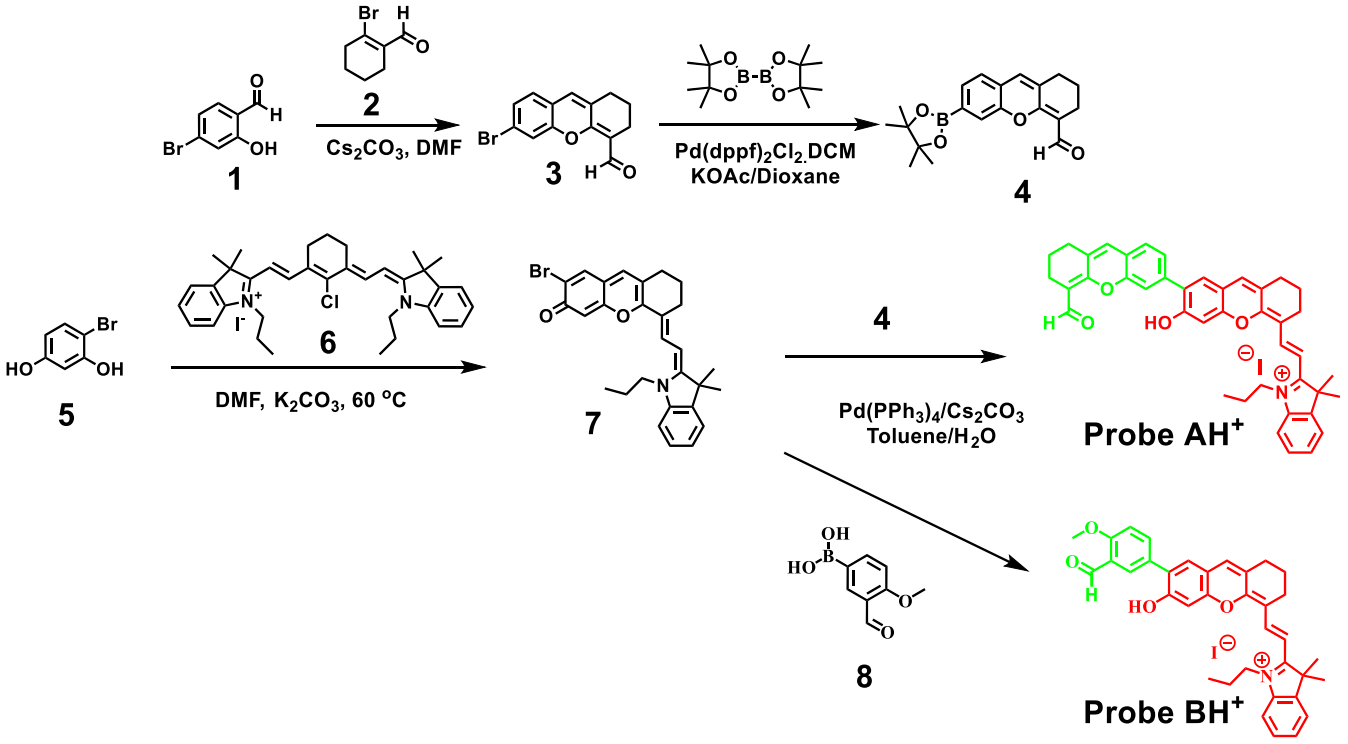

the cell culture medium containing 5% DMSO for 20 min, and then washed with PBS buffer three times. For monitoring different intracellular pH, the cells stained with probe **A** were further incubated for 20 min at 37 °C in different pH buffers containing 10 μM nigericin, which facilitates equilibrations between buffer pH and intracellular pH.[38−40,43,44,52−60] To investigate oxidative stress effects on intracellular pH fluctuations, the cells stained with probe **A** were further incubated with redox-active chemicals such as different concentrations of 100 μM hydrogen peroxide, 10 μM FCCP (carbonyl cyanide 4-(trifluoromethoxy)phenylhydrazone), and 1 mM NAC (*N*-acetylcysteine) for 30 min in pH 7.4 PBS buffer. Fluorescence cellular imaging was conducted to collect near-infrared fluorescence (750−800 nm). The cytotoxicity of the probe on HeLa cells was obtained via an MTT assay according to the manufacturer's guidelines.[38−40,43,44,52−60]

2.5. Theoretical Calculations. Optimization and frequency calculations were conducted at the APFD/6-311+G(d) level using the Gaussian 16[61] suite of programs. Imaginary frequencies were not obtained. The first ten excited states were assessed based on TD-DFT optimizations[62] in a Polarizable Continuum Model (PCM) of water.[63] Results were interpreted using GausView[64] for all other data and figures. *XYZ* coordinates and specific conditions for the pK_a calculations are detailed in Supporting Information.

3. RESULTS AND DISCUSSION

3.1. Probe Synthesis. We systematically engineered a novel hemicyanine derivative by integrating a formyl-functionalized xanthene moiety into the hemicyanine framework (Scheme 2). The synthesis of probe **A** involved coupling compound 6-(4,4,5,5-tetramethyl-1,3,2-dioxaborolan-2-yl)-2,3-dihydro-1H-xanthene-4-carbaldehyde, **4**, with hemicyanine dye, 7, via a palladium-catalyzed Suzuki reaction.[65] Intermediate **4** was obtained through a similar palladium-catalyzed Suzuki reaction between 6-bromo-2,3-dihydro-1H-xanthene-4-carbaldehyde, **3**, and 4,4,4′,4′,5,5,5′,5′-octamethyl-2,2′-bi-(1,3,2-dioxaborolane). The hemicyanine dye, 7, was prepared by subjecting cyanine dye (IR-780), **6**, to a reaction with 4-bromobenzene-1,3-diol under basic conditions. Probe **B** was obtained by coupling **4** with (3-formyl-4-methoxyphenyl)-boronic acid, **8**, also via a palladium-catalyzed Suzuki reaction. The hemicyanine platform has gained significant attention for its advantageous red to near-infrared emission, making it ideal for near-infrared imaging with minimal impact on cellular and tissue integrity. The incorporation of the xanthene core into the hemicyanine platform further fine-tuned the dye toward longer near-infrared wavelengths. Moreover, it enabled ratiometric monitoring of pH variations in particular with probe **B** through an Intramolecular Charge Transfer (ICT) mechanism, relying on the protonation and deprotonation of the probe's hydroxyl group as depicted in Scheme 1.

3.2. Probe Spectroscopic Investigations. The effect of changing the pH on the probes' optical properties was investigated using different pH buffer/dimethyl sulfoxide (v/v = 9:1) solutions. Probe **A** showed both absorption and fluorescence in the red to near-infrared region, i.e., longer than 650 nm, under acidic or basic conditions (Figure 1). Under a basic condition at pH 9.3, the probe exhibited a main absorption peak at 780 nm and a shoulder peak at 730 nm. Gradual pH decreases from 9.3 to 2.8 resulted in increases of the absorption peak at 780 nm, gradual decreases of the absorption peak at 730 nm, and the appearance of two additional absorption shoulder peaks at 680, and 630 nm. In a basic pH 9.3 buffer, the probe displayed fluorescence at 740 nm. Gradual acidification to pH 2.8 from 9.3 resulted in significant decreases of the fluorescence peak at 740 nm and triggered a new fluorescence peak at 780 nm which grew in intensity as the pH decreased from 9.3 to 2.8, indicating that the probe will be sensitive to detect pH changes. In contrast,

https://doi.org/10.1021/acsomega.4c07303
ACS Omega 2024, 9, 42049−42060

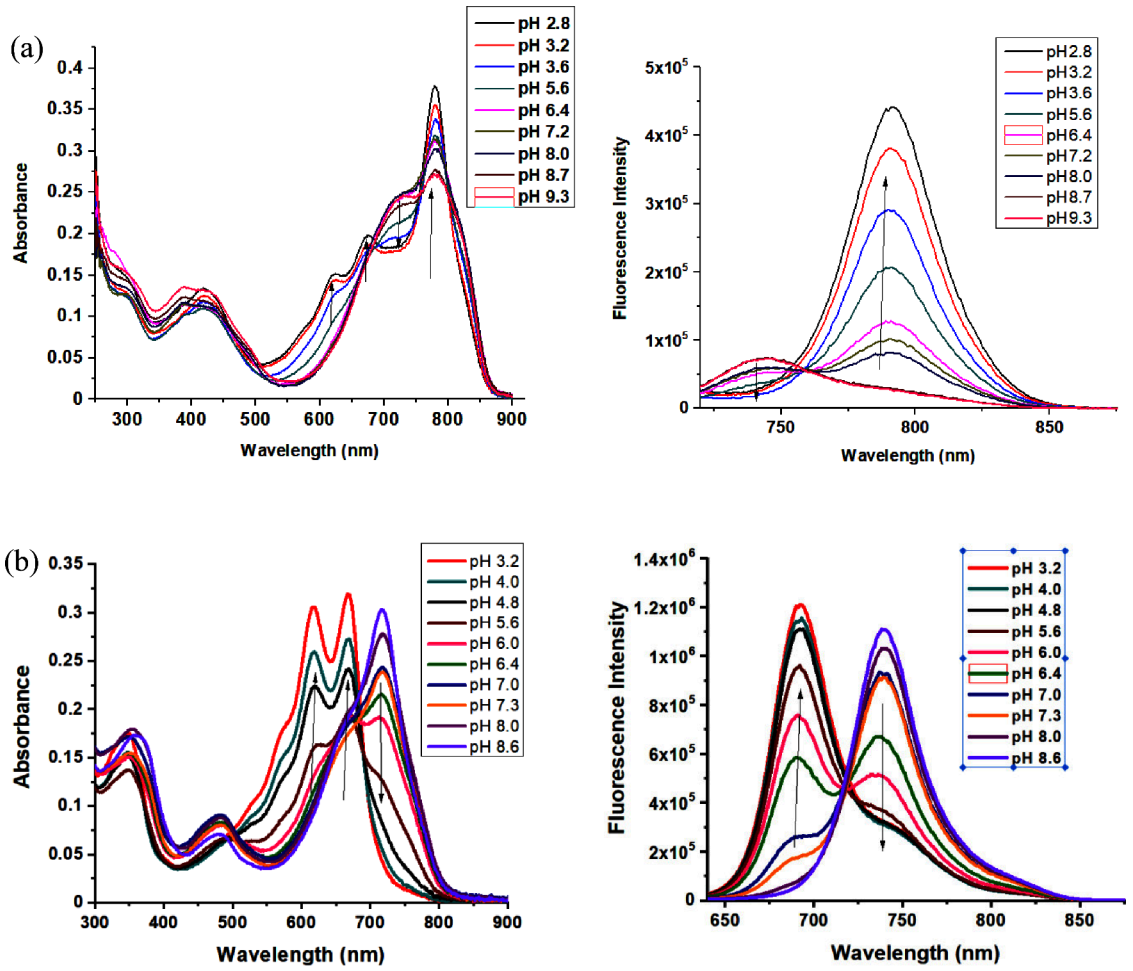

Figure 1. Absorbance (left) and fluorescence (right) spectra of 10 μM probe **A** (a) in buffers with different pH values containing 10% DMSO under excitation at 700 nm and 10 μM probe **B** (b) in pH buffers containing 30% DMSO under 620 nm excitation for probe **B**. Arrows indicate the direction of increased acidity.

probe **B** also displayed pH-dependent ratiometric absorptions (618 and 668 nm at pH 3.2; 717 nm at pH 8.6) and fluorescence (693 nm at pH 3.2; 739 at pH 8.6) in mostly the red to near IR region, Figure 1. The pH-dependent fluorescent spectra for probe **B** features one clear isosbestic point. An interesting difference between probes **A** and **B** is that the change in intensity of the fluorescent peaks was reversed, Figure 1 with the acidification and the peak at lower wavelengths for probe **B**, i.e., at 693 nm, were observed with much greater intensity, allowing for ratiometric measurements. Probe **A** possesses a pK_a value of 6.97, Figure S10, which was determined by using the Henderson−Hasselbalch equation. The fluorescent spectra for probe **B** provided data for two pK_a determinations with a value of 6.26 for the peak at 693 nm similar to the value of 6.54 for the peak at 739 nm, Figure S11.

3.3. Theoretical Calculations. Theoretical calculations (full details in Supporting Information) were conducted in order to assess if any changes in geometry would result from the protonation of probes. The probes each consisted of three planar aromatic sections. The plane based on the central aromatic section of the leftmost xanthene is at 43.25°, **A**; 43.46°, **B** to the equivalent central plane of the central xanthene whereas the plane of the indole moiety is only slightly twisted for **A** at 7.22°, and more twisted in **B** at 21.12° to the central xanthene plane. Upon protonation, the equivalent interplanar angles are 54.94, $\mathbf{AH^+}$; 59.13°, $\mathbf{BH^+}$ and 9.17°, $\mathbf{AH^+}$; 7.61°, $\mathbf{BH^+}$ respectively, which suggests that $\mathbf{AH^+}$ is in a similar conformation to probe **A** but $\mathbf{BH^+}$ has adopted a more planar conformation compared to **B** with respect to the central xanthene and indole moieties. This conformational similarity is displayed in an overlay diagram of the probes in Figure S20.

A selected listing of calculated bond distances is given in Table 1. This shows a decrease in the C−$O_{hydroxy}$ bond distance going from 1.3470 in probe $\mathbf{AH^+}$ to 1.2522 Å in **A** (1.34754 in probe $\mathbf{BH^+}$ to 1.25322 Å in **B**) concomitant with

Table 1. Comparison of Selected Bond Distances between Probes $\mathbf{AH^+}$ and A

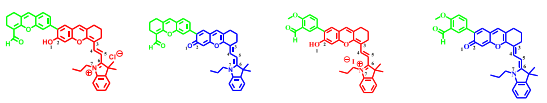

Probe	$\mathbf{AH^+}$	A	$\mathbf{BH^+}$	B
O_1-C_2	1.34700	1.25215	1.34754	1.25322
C_3-C_4	1.40393	1.38042	1.40356	1.37936
C_4-C_5	1.38699	1.40718	1.38654	1.40767
C_5-C_6	1.39711	1.38008	1.39655	1.37864
C_6-N_7	1.34368	1.35819	1.34354	1.35771

https://doi.org/10.1021/acsomega.4c07303
ACS Omega 2024, 9, 42049−42060

decreases in the C_3-C_4 and C_5-C_6 distances with slight increases in the C_4-C_5 and C_6-N_7 distances. This would suggest that the quinone conformer forms of both probes are responsible for the increase in the emission wavelength observed experimentally.

There were differences in the calculated absorptions at the APFD/6-311+G(d) level with probe **A** displaying a major absorption at 617 nm (expt. 730 and 780 nm), probe **AH**$^+$ at 558 nm (expt. 780 nm), probe **B** displaying a major absorption at 599 nm (expt. 668 and 717 nm), and probe **BH**$^+$ at 551 nm (expt. 739 nm). Using these optimized geometries and conducting the absorption calculation with the PBE1PBE[66] (**A**, 612.2; **AH**$^+$, 553.8 nm) and CAM-B3LYP[67] (**A**, 581.0; **AH**$^+$, 533.7 nm) resulted in a similar trend in these values. While both probe **A** and **AH**$^+$ absorb at 780 nm, Figure 1, new peaks for **AH**$^+$ were observed at 680 and 630 nm and presumably the calculations are reflective of this reality. A similar trend was noted for probe **B** which featured only one absorption at 717 nm under basic conditions but two for **BH**$^+$ at 618 and 668 nm at a pH of 3.2.

Inspection of the current density diagram in Figure 2 indicates that the electronic transition originates from the

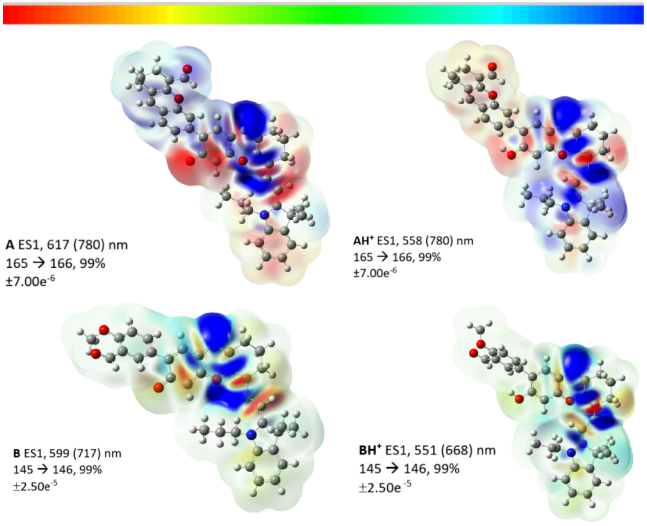

Figure 2. Current density difference drawings as isosurfaces of probes **A** (top left) and **AH**$^+$ (top right) and probes **B** (bottom left) and **BH**$^+$ (bottom right). The number of excited states (ES), the calculated (and experimental) wavelengths, and the transitions together with percentage contributions are listed. The range values for the color scale illustrated at the top of the figure are also listed. Drawings of the numbered LCMOs are available in the Supporting Information.

indole moiety ending up in the central xanthene group for probe **A** and changes upon protonation in probe **AH**$^+$ originating from the top xanthene group onto the central one. In contrast, for probes **B** and **BH**$^+$ the transitions originate from the outer extremities of the molecules and end up on the central xanthene moiety. This difference in the origin of the transitions, probably due to the electron-donating methoxy group in probe **BH**$^+$, accounts for the differences noted between the intensities of the observed fluorescent peaks between probes **AH**$^+$ and **BH**$^+$, Figure 1. These absorptions occurred with large oscillating constants, Table S7 for **AH**$^+$ and S8 for **BH**$^+$, suggesting that they should be experimentally observed. It is possible that the rigidity afforded by delocalization of electron density in the ethyl link, see Scheme 1, connecting the middle xanthene to the indole group results in less loss of fluorescence via nonradiative mechanisms with probes **AH**$^+$ and **BH**$^+$ and the observed increase in intensity, Figure 1. Notably probe **BH**$^+$ was calculated to have a slightly more planar arrangement between the indole and central xanthene moieties, compared to probe **AH**$^+$. This may also contribute to the greater intensity observed in the fluorescence spectra for the two peaks in probe **BH**$^+$, Figure 1.

Theoretical calculations for the pK_a value for probe **A**, where the Gibbs free energy values were obtained from the application of the functionals, basis sets and conditions detailed in Table 2 (coordinates in Supporting Information), were obtained using eq 1.[68] We find that similar results are obtained using the CAM-B3LYP[67] (pK_a = 3.11) and APFD[69] (pK_a = 3.41) functionals with

$$pK_a = ((G_{aq}\mathbf{A} - G_{aq}\mathbf{AH}) + (G_{aq}\mathbf{H})/(2.303^{*}RT) \quad (1)$$

6-311+(d) basis sets and the addition of water using the self-consistent reaction field (SCRF) where the solvent is modeled as a "continuous uniform dielectric medium".[70] However, these results differ substantially from the experimental value, i.e., pK_a = 6.97. Adding one water molecule and applying the functional M06-2X utilized for pK_a calculations[68] in a series of carboxylic acids, amines and thiols with the solvation model based on density (i.e., SMD) resulted in a calculated pK_a value of 9.02, Table 2. Employing the CAM-B3LYP functional with an identical basis set on the probes without the added water molecule resulted in a pK_a value of 9.57 illustrating the contribution of this SMD approach. Interestingly, employing more diffuse functions i.e., the 6-311+g(d,p) basis set, resulted in values of 6.33 and 8.26 for the IEFPCM and SMD conditions respectively, Table 2. Furthermore, adding one molecule of water to the probe situated hydrogen bonded to the phenoxide O atom resulted in pK_a values of 6.09 (IEFPCM) and 4.51 (SMD), Table 2. As noted previously the inclusion of a water molecule may be useful when the SCRF model is employed for aqueous systems being studied.[71] We can conclude that the inclusion of the water molecule coupled with the condition SMD, SAS, α = 0.485 did not result in an acceptable pK_a value for probe **A**. The closest agreement at pK_a = 6.33 to experimental at pK_a = 6.97 was with the probe without added water defined by the APFD/6-311+g(d,p)/IEFPCM, water combination conditions, Table 2. In order to determine if this approach would apply to phenols in general, the pK_a of phenol was determined using similar conditions, Table 2. Models involving just phenol and phenoxide at the APFD/6.311+g(d,p)/IEFPCM water condition resulted in a pK_a value of 17.12. Employing an APFD/6.31+g(d,p)/SMD approach resulted in a lower value of 13.65 but increasing the basis set to 6.311+g(d,p) resulted in 14.26. This closest pK_a value to the experimentally determined one of 9.98[72] was calculated at 11.97 for phenol•H_2O using the APFD/6.311+g(d,p)/SMD condition. Given the closer agreement between calculated and experimental pK_a values for probe **A** with the APFD/6-311+g(d,p)/IEFPCM water condition, calculations on other molecules are required to determine the general applicability of these approaches in calculating the pK_a for phenols. Interestingly, employing just the APFD/6-311+g(d,p)/ IEFPCM, water combination condition without added water molecules for probe **B** resulted in a calculated pK_a value of 6.41, Table 2, in between those observed

https://doi.org/10.1021/acsomega.4c07303
ACS Omega 2024, 9, 42049−42060

Table 2. Theoretical Calculations of pK_a for Probes A, B, and Phenol

molecule/table	functional/basis set	condition, SCRF	G(A) Hartrees	G(AH) Hartrees	pK_a
A/S9 and $\mathbf{AH^+}$/S10	CAM-B3LYP/6-311+g(d)	IEFPCM, water	−1978.366856	−1978.804363	3.11
A/S1 and $\mathbf{AH^+}$/S5	APFD/6-311+g(d)	IEFPCM, water	−1977.841169	−1978.279336	3.41
A•H_2O/S11 and $\mathbf{AH^+}$•H_2O/S12	M06-2X/6-31+G(d,p)	SMD, SAS, α = 0.485	−2054.669442	−2055.11981	9.02
A/S13 and $\mathbf{AH^+}$/S14	CAM-B3LYP/6-31+g(d)	SMD, SAS, α = 0.485	−1978.048156	−1978.499707	9.57
A/S15 and $\mathbf{AH^+}$/S16	APFD/6-311+g(d,p)	IEFPCM, water	−1977.897741	−1978.342251	6.33
A/S17 and $\mathbf{AH^+}$/S18	APFD/6-311+g(d,p)	SMD, SAS, α = 0.485	−1977.906169	−1978.354887	8.26
A•H_2O/S19 and $\mathbf{AH^+}$•H_2O/S20	APFD/6-311+g(d,p)	IEFPCM, water	−2054.298992	−2054.742992	6.09
A•H_2O/S21 and $\mathbf{AH^+}$•H_2O/S22	APFD/6-311+g(d,p)	SMD, SAS, α = 0.485	−2054.316147	−2054.756711	4.51
phenol/phenoxide/S23	APFD/6-311+g(d,p)	IEFPCM, water	−306.760330	−307.228317	17.12
phenol/phenoxide/S24	APFD/6-31+g(d,p)	SMD, SAS, α = 0.485	−306.801082	−307.261509	13.65
phenol/phenoxide/S25	APFD/6-311+g(d,p)	SMD, SAS, α = 0.485	−306.767446	−307.229199	14.26
phenol•H_2O/phenoxide•H_2O/S26	APFD/6-311+g(d,p)	SMD, SAS, α = 0.485	−383.169523	−383.626307	11.97
B/S4 and $\mathbf{BH^+}$/S6	APFD/6-311+g(d,p)	IEFPCM, water	−1747.038651	−1747.483349	6.41

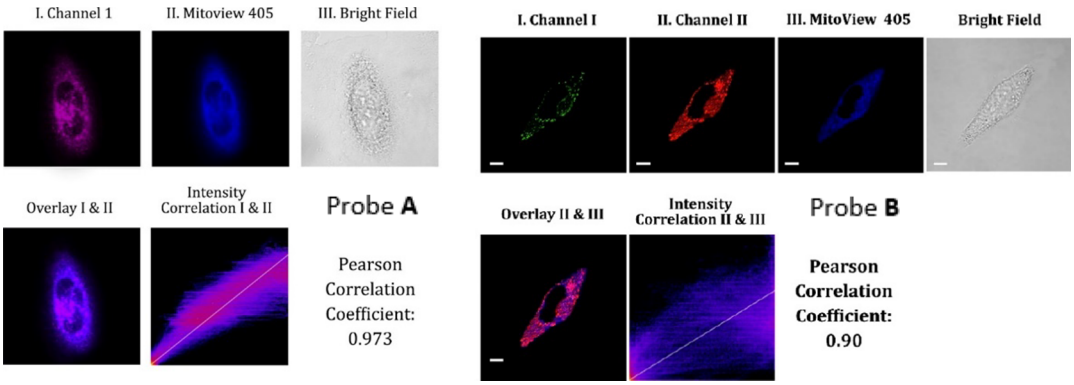

Figure 3. Fluorescence images of HeLa cells incubated with 10 μM probe **A** and 5 μM of Mitoview 405 30 min (left) and incubated for 20 min with 10 μM of MitoView 405 dye and probe **B** (10 μM) (right). For **A**, the near-infrared fluorescence (750−800 nm) of the probe was collected under excitation at 633 nm while the fluorescence (450−500 nm) of Mitoview 405 under excitation at 405 nm. For **B**, the fluorescence images of channel I were collected from 650 to 700 nm and fluorescence images of channel II were collected from 750 to 800 nm at 633 nm excitation with scale bars at 20 μM. Channel III was collected from 425 to 475 nm at 405 nm excitation with scale bars at 20 μM.

experimentally for the two fluorescent peaks at 6.26 and 6.54, Figure S11.

3.4. Probe Photostability Study. Photostability is a crucial attribute of the probe's effectiveness in practical cellular imaging applications. To assess its photostability, fluorescence intensities were measured at 780 nm in pH 3.6 and 7.4 buffers, utilizing a 700 nm excitation source over 2 h for probe **A**, and, in pH 7.0 buffer at 693 and 739 nm under excitation at 620 nm for probe **B** (see Figure S12). Impressively, the fluorescence intensities of these probes remained at over 96% of the initial value even after a 2 h exposure to radiation, underscoring their robust photostability characteristics.

3.5. Probe Reversibile Responeses to pH Changes. We conducted an assessment to determine the responsiveness to pH fluctuations with probe **A** by monitoring its fluorescence intensity at 780 nm while repetitively adjusting the pH between 8.0 and 3.6, Figure S13. The results unequivocally reveal the probe's ability to exhibit reversible fluorescence responses to cyclic pH variations between 3.6 and 8.0. This not only underscores the probe's excellent pH reversibility but also highlights its remarkable reproducibility and chemical structure robustness, as evidenced by the consistent and invariant fluorescence intensities throughout the pH adjustment process.

3.6. Probe Selectivity Evaluation. The selectivity for probes **A** and **B** was investigated employing different biological species such as cations (Na^+, Sn^{2+}, Fe^{3+}, Zn^{2+}, Mg^{2+}, Ca^{2+}, Cu^+, K^+), anions (HS^-, HSO_3^-, Cl^-, NO_3^-, SO_3^{2-}, IO_3^-, HCO_3^-, SO_4^{2-}, PO_4^{3-}, CO_3^{2-}), and various amino acids in pH 4.0 and pH 7.4 buffers (probe **A**, Figures S14−S16; probe **B**, Figure S17). Significant differences with the fluorescence signals in pH 4.4 and 7.4 buffers for probe **A** containing these species were not observed, indicating that this probe exhibited highly selective responses to pH without any considerable interference from the biological setting, Figures S14−S16. The emission intensities of probe **B** did not change significantly in the absence and presence of different cations (100 μM), anions (100 μM), and amino acids (100 μM) in pH 7.0 buffer under excitation at 620 nm, Figure S17.

3.7. Evaluation of the Probe Cytotoxicity. Before applying the probe for cellular imaging, we evaluated its cytotoxicity on probes **A** and **B** using the MTT assay with HeLa cells, Figure S18. Encouragingly, the probes demonstrated low cytotoxicity and excellent biocompatibility, as evidenced by cell viability exceeding 80% for probe **A** and 75% for probe **B**, even at high probe concentrations of 50 μM.

3.8. Cellular Imaging of Intracellular pH Changes. Hemicyanine dyes carrying positive charge residues have previously been reported to selectively stain mitochondria in live cells, primarily through electrostatic interactions with the negatively charged internal mitochondrial membrane.[73] Given this established mechanism, we anticipated that our probes, featuring a positive charge due to the incorporation of the formyl-functionalized moieties, xanthene for probe **A** and methoxybenzaldehyde for **B**, would maintain the same

https://doi.org/10.1021/acsomega.4c07303
ACS Omega 2024, 9, 42049−42060

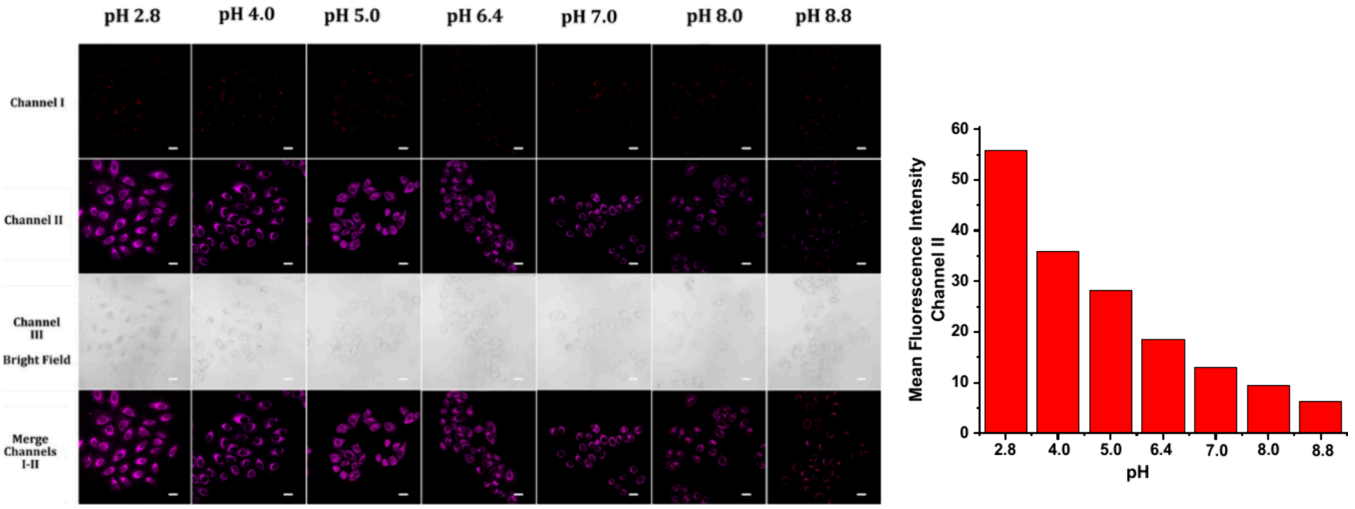

Figure 4. Fluorescence images (left) of HeLa cells incubated with 10 μM of probe **A** in different pH buffers containing 5 μM nigericin. The fluorescence images of channel I were collected from 700 to 750 nm and fluorescence images of channel II were collected from 750 to 800 nm for probe **A** under excitation at 633 nm. Histogram (right) for fluorescence intensity of probe **A** (10 μM) at different pH levels.

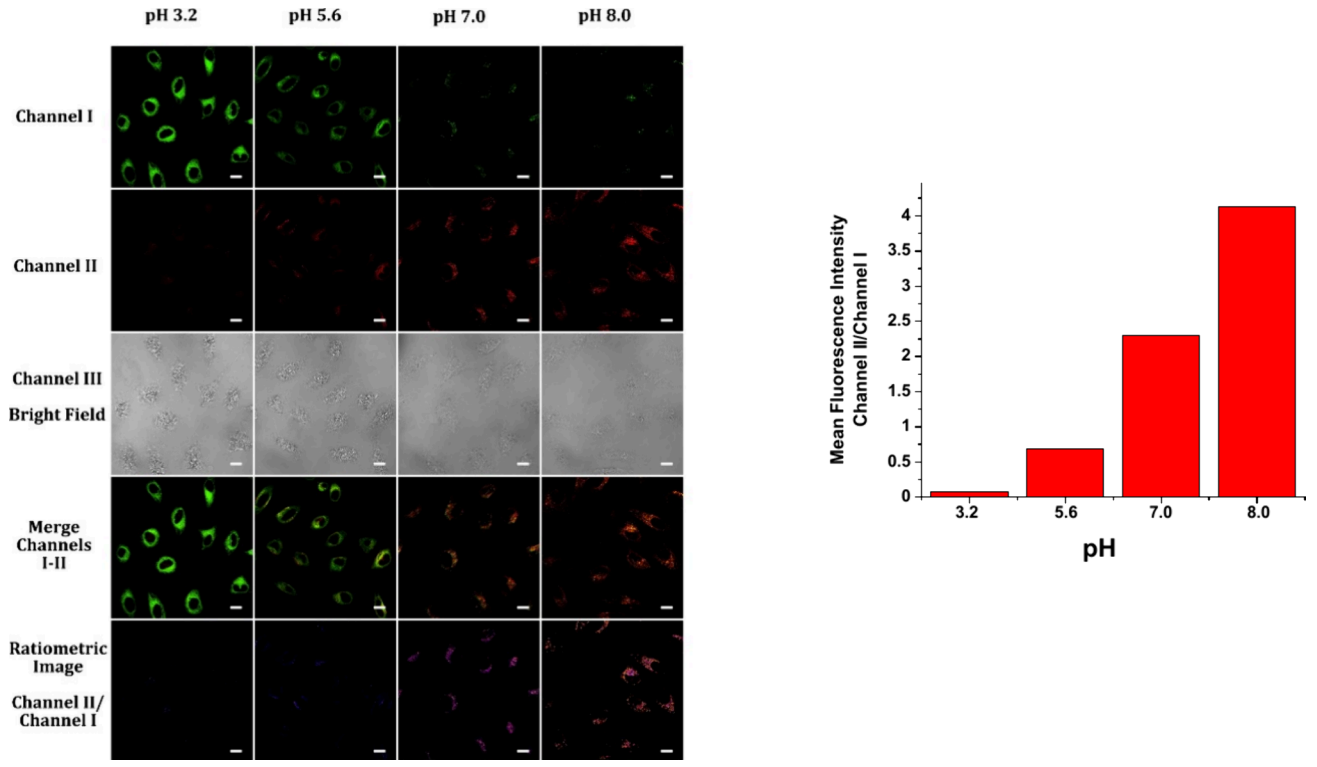

Figure 5. Fluorescence images (left) of HeLa cells incubated with probe **B** (10 μM) in different pH buffers containing 5 μM nigericin for 20 min. The fluorescence images of channel I were collected from 650 to 700 nm and fluorescence images of channel II were collected from 750 nm to 800 for probe **B** at 633 nm excitation with scale bars at 50 μM. Histogram (right) for fluorescence intensity of probe **B** (10 μM) in channel II at different pH levels.

distinctive mitochondrial targeting capability. To test our hypothesis regarding the probe's specificity for mitochondria, we conducted a colocalization experiment, costaining HeLa cells with our probes and a commercially available mitochondria-specific stain, MitoView 405. The remarkable Pearson's colocalization coefficients of 0.973 and 0.90 between probes **A** and **B** respectively and MitoView 405, Figure 3, provided unequivocal confirmation of both probe's exceptional specificity for mitochondria.

We further elevated whether the probe could be used to quantify intracellular pH changes in live cells by incubating the probe-stained HeLa cells with nigericin, a K^+ for H^+ exchange carboxylic ionophore,[74] in different pH buffers, (probe **A**, Figure 4; probe **B**, Figure 5) by conducting fluorescence cellular imaging because nigericin has been commonly employed to adjust intracellular pH to environmental buffer pH.[38−40,43,44,52−60] With probe **A**, decreasing the intracellular pH from 8.8 to 2.8 led to gradual enhancements in the intensity of the near-infrared fluorescence of the cells in the

https://doi.org/10.1021/acsomega.4c07303
ACS Omega 2024, 9, 42049−42060

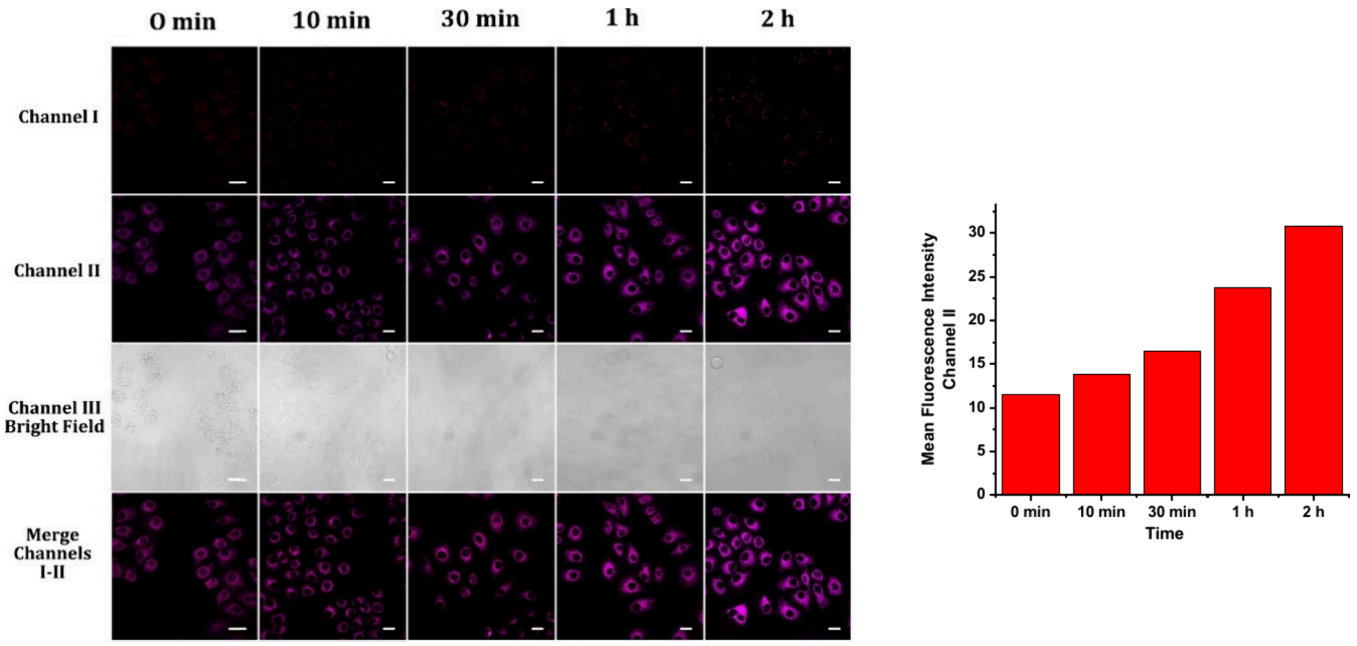

Figure 6. Fluorescence images (left) of HeLa cells incubated with 10 μM of probe **A** in serum-free medium for different times. The fluorescence images of channel I were collected from 700 to 750 nm and fluorescence images of channel II were collected from 750 to 800 nm for probe **A** under excitation at 633 nm. Histogram (right, channel II) for fluorescence intensity of probe **A** (10 μM) at different time intervals.

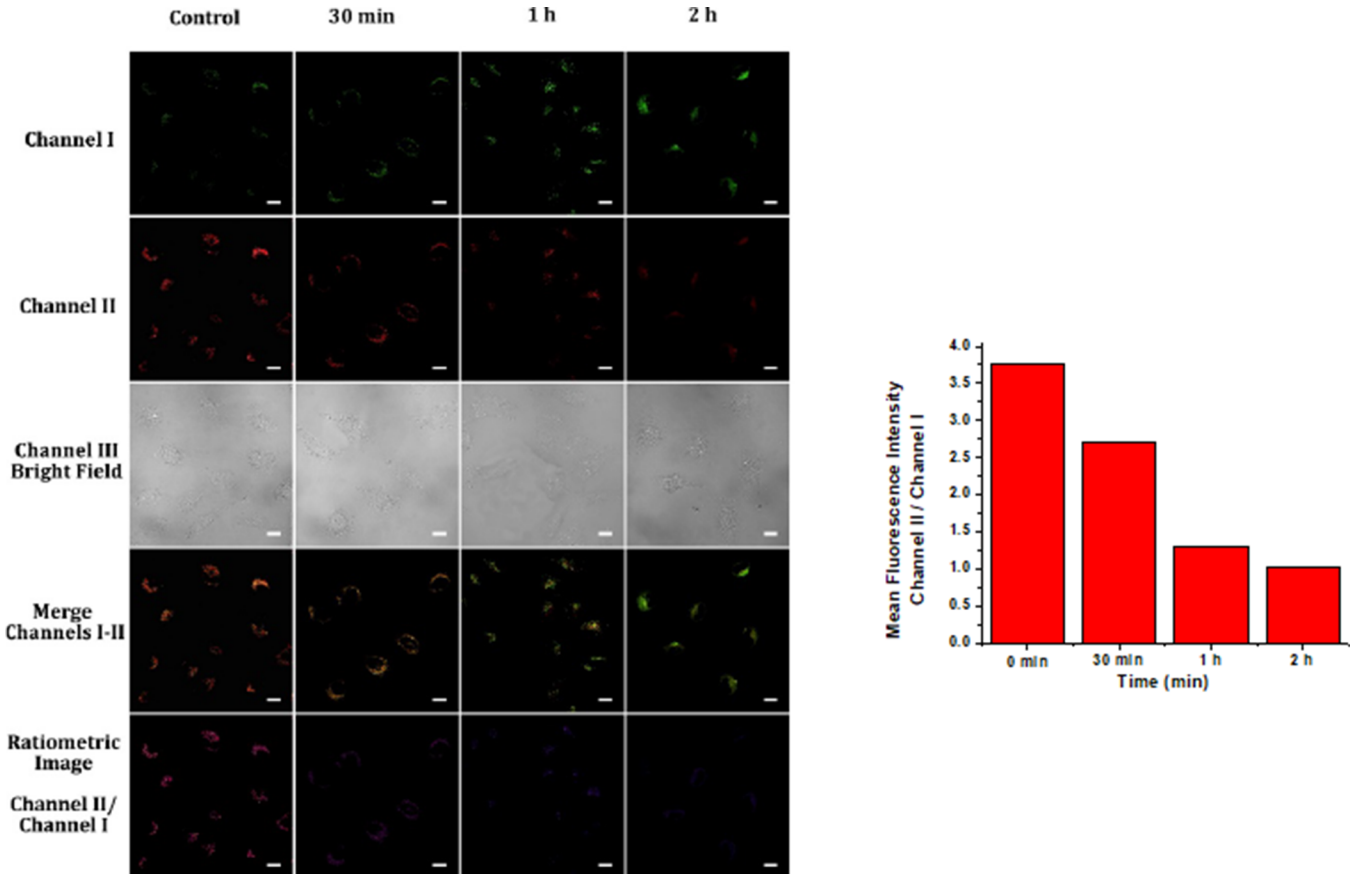

Figure 7. Fluorescence images (left) of HeLa cells including probe **B** (10 μM) in serum-free medium for different periods. The fluorescence images of channel I were collected from 650 to 700 nm and fluorescence images of channel II were collected from 750 nm to 800 for probe **B** at 633 nm excitation with scale bars at 50 μM. Histogram (right, channel II) for fluorescence intensity of probe **B** (10 μM) at different time intervals.

range 700 to 750 nm, Figure 4, showing intracellular pH-dependent fluorescence responses, similar to what was observed in the fluorescence responses pattern in the study on its optical properties, Figure 1. For probe **B**, both channel I

https://doi.org/10.1021/acsomega.4c07303
ACS Omega 2024, 9, 42049−42060

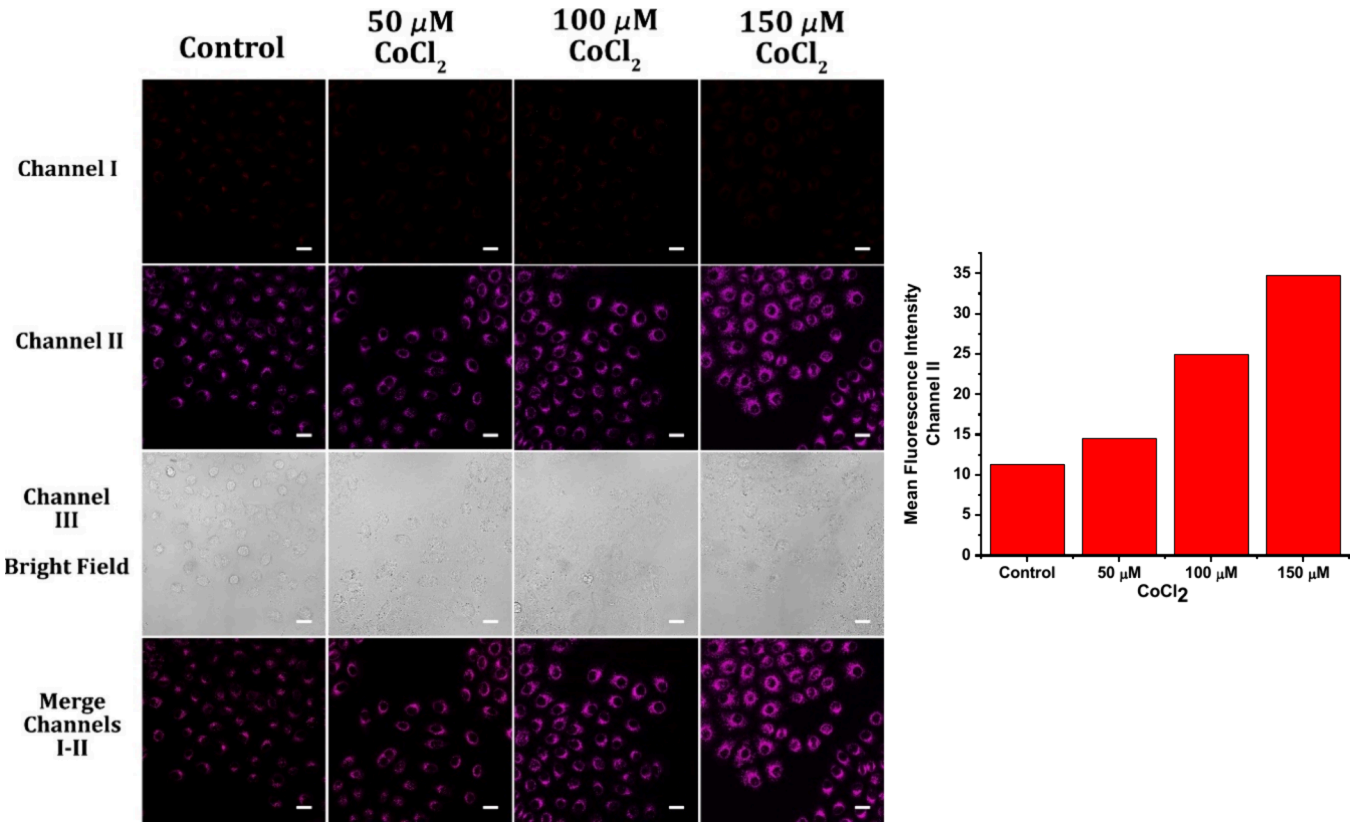

Figure 8. Fluorescence images (left) of HeLa cells incubated with 10 μM of probe **A** in different concentrations of $CoCl_2$. The fluorescence images of channel I were collected from 700 to 750 nm and fluorescence images of channel II were collected from 750 to 800 nm for probe **A** under excitation at 633 nm. Histogram (right, channel II) for fluorescence intensity of probe **A** (10 μM) at different concentrations of $CoCl_2$.

and II could be employed and we show the decrease in fluorescence, Figure 5, as the pH changed from 8.0 to 3.2 in channel II, 750 to 800 nm. These results convincingly demonstrate that both probes are capable of quantitative monitoring of intracellular pH changes.

Probe **A** was also applied to monitor intracellular pH fluctuations under oxidative stress, achieved through the chemical treatment of HeLa cells with 10 μM FCCP, 1 mM NAC, and 100 μM hydrogen peroxide, Figure S19. Upon FCCP treatment, a notable increase in intracellular fluorescence intensity was observed, signifying mitochondrial acidification, Figure S19. This outcome is attributed to FCCP's disruption of the mitochondrial membrane potential, leading to mitochondrial acidosis. Similarly, treatment with NAC, a proton donor, intensified cellular fluorescence intensity, resulting in mitochondrial acidification, Figure S19. NAC's action accomplishes the acidification of mitochondria. Furthermore, the introduction of hydrogen peroxide, known to impede cell metabolism and induce oxidative damage to living cells,[75] also resulted in enhanced cellular fluorescence. This enhancement triggers mitochondrial acidosis, as hydrogen peroxide facilitates the redistribution of proton ions to mitochondria from acidified organelles by weakening the vacuolar proton pump (V-ATPase).

Nutrient deprivation results in mitochondria dysfunction and triggers a mitophagy process which eliminates dysfunctional mitochondria resulting in a more acidic environment within.[44,51,58,76,77] We also evaluated the feasibility of using both probes to monitor mitophagy induced by nutrient starvation of HeLa cells in a serum-free medium. Cellular fluorescence intensities of the probes in HeLa cells increased with incubation times during the cell nutrient starvation in a serum-free medium, indicating that mitophagy results in a gradual pH decrease which correlates with the cell starvation time, probe **A**, Figure 6; probe **B**, Figure 7.[44,51,58,76,77] These results demonstrate the applicability of the probes in monitoring starvation-stimulated mitophagy in live cells.

We further used probe **A** to detect pH changes during the hypoxia process of HeLa induced by $CoCl_2$ treatment.[78−80] Chemical hypoxia of cells induced by $CoCl_2$ treatment is a convenient and well-known approach that is commonly used in the biology fields.[78−80] Probe **A**-stained HeLa cells showed considerable fluorescence enhancements under chemical hypoxia generated by $CoCl_2$ treatment, Figure 8. Cellular fluorescence signals intensified with increases in the concentration of $CoCl_2$, indicating that the probe can track a normoxia to a hypoxia transition within cells induced by this treatment by reacting to pH changes during cell acidification as a result of hypoxia.

4. CONCLUSIONS

In summary, our study involved the strategic design and synthesis of near-infrared fluorescent probes by introducing formyl-functionalized xanthene and methoxybenzene moieties onto a xanthene-hemocyanin framework. This modification achieved a significant shift in the probe's emission toward the longer near-infrared region and facilitated pH-dependent ratiometric fluorescence responses. The results of theoretical calculations afforded an understanding of the changes in bond distances as a result of deprotonation and the (APFD/6-

https://doi.org/10.1021/acsomega.4c07303
ACS Omega 2024, 9, 42049−42060

311+G(d,p)/IEFPCM, water) combination of functional, basis set, and solvent condition allowed for the calculation of the pK_a values close to those obtained experimentally. Importantly, the probes exhibited exceptional cell permeability, excellent biocompatibility, and a remarkable specificity for targeting mitochondria. Its successful application allowed us to monitor changes in mitochondrial pH levels under conditions of oxidative stress, hypoxia, and during mitophagy. Leveraging the versatile formyl residue within this adaptable platform, we are actively pursuing the creation of a series of ratiometric near-infrared pH-responsive fluorescent probes. This is achieved by reacting the formyl group with a diverse array of electron-withdrawing functional building blocks, effectively extending the near-infrared fluorescence of hemicyanine dyes into wavelengths exceeding 900 nm, even encompassing the second near-infrared window. Furthermore, we anticipate extending this methodology to modify the hydroxyl group of the resulting hemicyanine dyes, incorporating sensing elements for the sensitive and ratiometric quantitation of various analytes such as enzymes, biothiols, and hydrogen peroxide. These endeavors are currently under investigation and will be reported in due course.

■ ASSOCIATED CONTENT

Supporting Information

The Supporting Information is available free of charge at https://pubs.acs.org/doi/10.1021/acsomega.4c07303.

Synthesis of probe **A**, probe **B** and their precursors, ^{1}H NMR, ^{13}C NMR, and LCMS of probe **A** and probe **B**, effect on fluorescence with pH changes, photostability tests, fluorescence intensities of probe **A** and probe **B** in the presence and absence of cations, anions and amino acids, MTT assay, chemical tests with FCCP, NAC, and H_2O_2, and results of theoretical calculations (PDF)

■ AUTHOR INFORMATION

Corresponding Authors

Haiying Liu − *Department of Chemistry, Michigan Technological University, Houghton, Michigan 49931, United States;* orcid.org/0000-0001-8351-2017; Email: hyliu@mtu.edu

Rudy L. Luck − *Department of Chemistry, Michigan Technological University, Houghton, Michigan 49931, United States;* orcid.org/0000-0001-5436-1942; Email: rluck@mtu.edu

Authors

Sushil K. Dwivedi − *Department of Chemistry, Michigan Technological University, Houghton, Michigan 49931, United States*

Dilka Liyana Arachchige − *Department of Chemistry, Michigan Technological University, Houghton, Michigan 49931, United States*

Adenike Mary Olowolagba − *Department of Chemistry, Michigan Technological University, Houghton, Michigan 49931, United States*

Mohamed Mahmoud − *Department of Chemistry, Michigan Technological University, Houghton, Michigan 49931, United States*

Subash Pandey − *Department of Chemistry, Michigan Technological University, Houghton, Michigan 49931, United States*

Tara Vohs − *Department of Chemistry, Michigan Technological University, Houghton, Michigan 49931, United States*

Complete contact information is available at: https://pubs.acs.org/10.1021/acsomega.4c07303

Notes

The authors declare no competing financial interest.

■ ACKNOWLEDGMENTS

This work was based on support received from the National Institute of General Medical Sciences, National Institutes of Health, through Award Number R15GM152969-01 to R.L.L. and H.L. The study was also assisted with partial sponsorship from the National Institute of General Medical Sciences, National Institutes of Health, through Award Numbers 2R15GM114751 for H.L. and R15 GM146206-01 for H.L. and R.L.L. Our appreciation also extends to the National Science Foundation for their financial support under award number 2117318 for the acquisition of a new NMR spectrometer. Computational calculations for the fluorescent probes were conducted utilizing a high-performance computing infrastructure based at Michigan Technological University.

■ REFERENCES

(1) Johansson, A. C.; Appelqvist, H.; Nilsson, C.; Kagedal, K.; Roberg, K.; Ollinger, K. Regulation of apoptosis-associated lysosomal membrane permeabilization. *Apoptosis* **2010**, *15* (5), 527−540.

(2) Turk, B.; Turk, V. Lysosomes as "Suicide Bags" in Cell Death: Myth or Reality? *J. Biol. Chem.* **2009**, *284* (33), 21783−21787.

(3) Stinchcombe, J.; Bossi, G.; Griffiths, G. M. Linking albinism and immunity: The secrets of secretory lysosomes. *Science* **2004**, *305* (5680), 55−59.

(4) Casey, J. R.; Grinstein, S.; Orlowski, J. Sensors and regulators of intracellular pH. *Nat. Rev. Mol. Cell Biol.* **2010**, *11* (1), 50−61.

(5) Rizzolo, L. J.; Kornfeld, R. Post-Translational Protein Modification in the Endoplasmic-Reticulum - Demonstration of Fatty Acylase and Deoxymannojirimycin-Sensitive Alpha-Mannosidase Activities. *J. Biol. Chem.* **1988**, *263* (19), 9520−9525.

(6) Tan, J. Z. A.; Gleeson, P. A. Cargo Sorting at the trans-Golgi Network for Shunting into Specific Transport Routes: Role of Arf Small G Proteins and Adaptor Complexes. *Cells* **2019**, *8* (6), 531.

(7) Nilsson, T.; Au, C. E.; Bergeron, J. J. M. Sorting out glycosylation enzymes in the Golgi apparatus. *FEBS Lett.* **2009**, *583* (23), 3764−3769.

(8) Matsuyama, S.; Reed, J. C. Mitochondria-dependent apoptosis and cellular pH regulation. *Cell Death and Differentiation* **2000**, *7* (12), 1155−1165.

(9) Yue, Y. K.; Huo, F. J.; Lee, S.; Yin, C. X.; Yoon, J. A review: the trend of progress about pH probes in cell application in recent years. *Analyst* **2017**, *142* (1), 30−41.

(10) Xue, F. F.; Wen, Y.; Wei, P.; Gao, Y. L.; Zhou, Z. G.; Xiao, S. Z.; Yi, T. A smart drug: a pH-responsive photothermal ablation agent for Golgi apparatus activated cancer therapy. *Chem. Commun.* **2017**, *53* (48), 6424−6427.

(11) Taguchi, T. Emerging roles of recycling endosomes. *J. Biochem.* **2013**, *153* (6), 505−510.

(12) Kobayashi, T.; Tanaka, T.; Toyama-Sorimachi, N. How do cells optimize luminal environments of endosomes/lysosomes for efficient inflammatory responses? *J. Biochem.* **2013**, *154* (6), 491−499.

(13) Wen, Y.; Zhang, W.; Liu, T.; Huo, F.; Yin, C. Pinpoint Diagnostic Kit for Heat Stroke by Monitoring Lysosomal pH. *Anal. Chem.* **2017**, *89* (21), 11869−11874.

(14) Zhang, T.; Huo, F.; Zhang, W.; Chao, J.; Yin, C. Ultra-pH-sensitive sensor for visualization of lysosomal autophagy, drug-

induced pH alteration and malignant tumors microenvironment. *Sens. Actuators B Chem.* **2021**, *345*, No. 130393.
(15) Rivinoja, A.; Pujol, F. M.; Hassinen, A.; Kellokumpu, S. Golgi pH, its regulation and roles in human disease. *Annals of Medicine* **2012**, *44* (6), 542−554.
(16) Kogot-Levin, A.; Zeigler, M.; Ornoy, A.; Bach, G. Mucolipidosis Type IV: The Effect of Increased Lysosomal pH on the Abnormal Lysosomal Storage. *Pediatr. Res.* **2009**, *65* (6), 686−690.
(17) Dupere-Minier, G.; Hamelin, C.; Desharnais, P.; Bernier, J. Apoptotic volume decrease, pH acidification and chloride channel activation during apoptosis requires CD45 expression in HPB-ALL T cells. *Apoptosis* **2004**, *9* (5), 543−551.
(18) Ko, M.; Quinones-Hinojosa, A.; Rao, R. J. Emerging links between endosomal pH and cancer. *Cancer and Metastasis Reviews* **2020**, *39* (2), 519−534.
(19) Reshkin, S. J.; Cardone, R. A.; Harguindey, S. Na+-H+ Exchanger, pH Regulation and Cancer. *Recent Pat. Anti-Cancer Drug Discovery* **2013**, *8* (1), 85−99.
(20) Zheng, T. Y.; Jaattela, M.; Liu, B. pH gradient reversal fuels cancer progression. *Int. J. Biochem. Cell Biol.* **2020**, *125*, No. 105796.
(21) Tipping, K. W.; Karamanos, T. K.; Jakhria, T.; Iadanza, M. G.; Goodchild, S. C.; Tuma, R.; Ranson, N. A.; Hewitt, E. W.; Radford, S. E. pH-induced molecular shedding drives the formation of amyloid fibril-derived oligomers. *Proc. Natl. Acad. Sci. U. S. A.* **2015**, *112* (18), 5691−5696.
(22) Lyros, E.; Ragoschke-Schumm, A.; Kostopoulos, P.; Sehr, A.; Backens, M.; Kalampokini, S.; Decker, Y.; Lesmeister, M.; Liu, Y.; Reith, W.; Fassbender, K. Normal brain aging and Alzheimer's disease are associated with lower cerebral pH: an in vivo histidine H-1-MR spectroscopy study. *Neurobiology of Aging* **2020**, *87*, 60−69.
(23) Lee, M. H.; Park, N.; Yi, C.; Han, J. H.; Hong, J. H.; Kim, K. P.; Kang, D. H.; Sessler, J. L.; Kang, C.; Kim, J. S. Mitochondria-Immobilized pH-Sensitive Off-On Fluorescent Probe. *J. Am. Chem. Soc.* **2014**, *136* (40), 14136−14142.
(24) Le Guern, F.; Mussard, V.; Gaucher, A.; Rottman, M.; Prim, D. Fluorescein Derivatives as Fluorescent Probes for pH Monitoring along Recent Biological Applications. *Int. J. Mol. Sci.* **2020**, *21* (23), 9217.
(25) Hou, J. T.; Ren, W. X.; Li, K.; Seo, J.; Sharma, A.; Yu, X. Q.; Kim, J. S. Fluorescent bioimaging of pH: from design to applications. *Chem. Soc. Rev.* **2017**, *46* (8), 2076−2090.
(26) Yin, J.; Hu, Y.; Yoon, J. Fluorescent probes and bioimaging: alkali metals, alkaline earth metals and pH. *Chem. Soc. Rev.* **2015**, *44* (14), 4619−4644.
(27) Chen, W. J.; Ma, X. X.; Chen, H. J.; Liu, S. H.; Yin, J. Fluorescent probes for pH and alkali metal ions. *Coord. Chem. Rev.* **2021**, *427*, No. 213584.
(28) Swanson, S. J.; Choi, W. G.; Chanoca, A.; Gilroy, S. In Vivo Imaging of Ca2+, pH, and Reactive Oxygen Species Using Fluorescent Probes in Plants. *Annu. Rev. Plant Biol.* **2011**, *62*, 273−297.
(29) Wang, R.; Yu, C. W.; Yu, F. B. A.; Chen, L. X. Molecular fluorescent probes for monitoring pH changes in living cells. *TrAC Trends Anal. Chem.* **2010**, *29* (9), 1004−1013.
(30) Dembska, A.; Bielecka, P.; Juskowiak, B. pH-Sensing fluorescence oligonucleotide probes based on an i-motif scaffold: a review. *Analytical Methods* **2017**, *9* (43), 6092−6106.
(31) Grillo-Hill, B. K.; Webb, B. A.; Barber, D. L. Ratiometric Imaging of pH Probes. *Methods Cell Biol.* **2014**, *123*, 429−448.
(32) Banik, D.; Manna, S. K.; Maiti, A.; Mahapatra, A. K. Recent Advancements in Colorimetric and Fluorescent pH Chemosensors: From Design Principles to Applications. *Crit. Rev. Anal. Chem.* **2023**, *53*, 1313−1373.
(33) Chen, Y. Recent advances in fluorescent probes for extracellular pH detection and imaging. *Anal. Biochem.* **2021**, *612*, No. 113900.
(34) Hande, P. E.; Shelke, Y. G.; Datta, A.; Gharpure, S. J. Recent Advances in Small Molecule-Based Intracellular pH Probes. *ChemBioChem* **2022**, *23*, No. e202100448.
(35) Gong, S. H.; Zhang, X.; Li, N.; Tang, B. Recent Progress of Fluorescent Nanoprobes for Organelle pH Detection. *Chem. J. Chin. Univ.* **2020**, *41* (9), 1933−1944.
(36) Wen, Y.; Jing, N.; Huo, F. J.; Yin, C. X. Recent progress of organic small molecule-based fluorescent probes for intracellular pH sensing. *Analyst* **2021**, *146* (24), 7450−7463.
(37) Zhang, T. X.; Xu, D.; Poon, C. Y.; Wang, X. L.; Bolze, F.; Li, H.; Wong, M. S. Tuning the pK(a) of two-photon bis-chromophoric probes for ratiometric fluorescence imaging of acidic pH in lysosomes. *Talanta* **2019**, *202*, 34−41.
(38) Zhang, Y. B.; Bi, J. H.; Xia, S.; Mazi, W.; Wan, S. L.; Mikesell, L.; Luck, R. L.; Liu, H. Y. A Near-Infrared Fluorescent Probe Based on a FRET Rhodamine Donor Linked to a Cyanine Acceptor for Sensitive Detection of Intracellular pH Alternations. *Molecules* **2018**, *23* (10), 2679.
(39) Wang, J. B.; Xia, S.; Bi, J. H.; Zhang, Y. B.; Fang, M. X.; Luck, R. L.; Zeng, Y. B.; Chen, T. H.; Lee, H. M.; Liu, H. Y. Near-infrared fluorescent probes based on TBET and FRET rhodamine acceptors with different pK(a) values for sensitive ratiometric visualization of pH changes in live cells. *J. Mater. Chem. B* **2019**, *7* (2), 198−209.
(40) Wan, S. L.; Xia, S.; Medford, J.; Durocher, E.; Steenwinkel, T. E.; Rule, L.; Zhang, Y. B.; Luck, R. L.; Werner, T.; Liu, H. Y. A ratiometric near-infrared fluorescent probe based on a novel reactive cyanine platform for mitochondrial pH detection. *J. Mater. Chem. B* **2021**, *9* (25), 5150−5161.
(41) Li, Y.; Wang, Y.; Yang, S.; Zhao, Y.; Yuan, L.; Zheng, J.; Yang, R. Hemicyanine-based High Resolution Ratiometric near-Infrared Fluorescent Probe for Monitoring pH Changes in Vivo. *Anal. Chem.* **2015**, *87* (4), 2495−2503.
(42) Lin, L. Y.; Zhao, J. J.; Zhang, L. L.; Huang, Y.; Ye, F. G.; Zhao, S. L. Real-time tracing the changes in the intracellular pH value during apoptosis by near-infrared ratiometric fluorescence imaging. *Chem. Commun.* **2018**, *54* (65), 9071−9074.
(43) Xia, S.; Fang, M. X.; Wang, J. B.; Bi, J. H.; Mazi, W.; Zhang, Y. B.; Luck, R. L.; Liu, H. Y. Near-infrared fluorescent probes with BODIPY donors and rhodamine and merocyanine acceptors for ratiometric determination of lysosomal pH variance. *Sensors and Actuators B-Chemical* **2019**, *294*, 1−13.
(44) Xia, S. A.; Wang, J. B.; Zhang, Y. B.; Whisman, N.; Bi, J. H.; Steenwinkel, T. E.; Wan, S. L.; Medford, J.; Tajiri, M.; Luck, R. L.; Werner, T.; Liu, H. Y. Ratiometric fluorescent probes based on through-bond energy transfer of cyanine donors to near-infrared hemicyanine acceptors for mitochondrial pH detection and monitoring of mitophagy. *J. Mater. Chem. B* **2020**, *8* (8), 1603−1615.
(45) Juvekar, V.; Lim, C. S.; Lee, D. J.; Song, D. H.; Noh, C. K.; Kang, H.; Shin, S. J.; Kim, H. M. Near-Infrared Ratiometric Two-Photon Probe for pH Measurement in Human Stomach Cancer Tissue. *ACS Appl. Bio Mater.* **2021**, *4* (3), 2135−2141.
(46) Mukherjee, A.; Saha, P. C.; Das, R. S.; Bera, T.; Guha, S. Acidic pH-Activatable Visible to Near-Infrared Switchable Ratiometric Fluorescent Probe for Live-Cell Lysosome Targeted Imaging. *ACS Sens.* **2021**, *6* (6), 2141−2146.
(47) Yuan, L.; Lin, W.; Zhao, S.; Gao, W.; Chen, B.; He, L.; Zhu, S. A Unique Approach to Development of Near-Infrared Fluorescent Sensors for in Vivo Imaging. *J. Am. Chem. Soc.* **2012**, *134* (32), 13510−13523.
(48) Wan, Q.; Chen, S.; Shi, W.; Li, L.; Ma, H. Lysosomal pH Rise during Heat Shock Monitored by a Lysosome-Targeting Near-Infrared Ratiometric Fluorescent Probe. *Angew. Chem., Int. Ed.* **2014**, *53* (41), 10916−10920.
(49) Li, X.; Hu, Y.; Li, X.; Ma, H. Mitochondria-Immobilized Near-Infrared Ratiometric Fluorescent pH Probe To Evaluate Cellular Mitophagy. *Anal. Chem.* **2019**, *91* (17), 11409−11416.
(50) Meng, Y.; Zhao, D.; Yang, X.; Li, Y.; Liu, B.; Zhang, Z.; Cui, S.; Wei, F. Near-Infrared Ratiometric Hemicyanine-Based pH Fluorescence Probe with Bone Targetability for Monitoring Bone Resorption. *Anal. Chem.* **2023**, *95* (7), 3736−3745.
(51) Li, X. Y.; Hu, Y. M.; Li, X. H.; Ma, H. M. Mitochondria-Immobilized Near-Infrared Ratiometric Fluorescent pH Probe To

https://doi.org/10.1021/acsomega.4c07303
ACS Omega 2024, 9, 42049−42060

Evaluate Cellular Mitophagy. *Anal. Chem.* **2019**, *91* (17), 11409−11416.
(52) Vegesna, G. K.; Janjanam, J.; Bi, J. H.; Luo, F. T.; Zhang, J. T.; Olds, C.; Tiwari, A.; Liu, H. Y. pH-activatable near-infrared fluorescent probes for detection of lysosomal pH inside living cells. *J. Mater. Chem. B* **2014**, *2* (28), 4500−4508.
(53) Fang, M. X.; Adhikari, R.; Bi, J. H.; Mazi, W.; Dorh, N.; Wang, J. B.; Conner, N.; Ainsley, J.; Karabencheva-Christova, T. G.; Luo, F. T.; Tiwari, A.; Liu, H. Y. Fluorescent probes for sensitive and selective detection of pH changes in live cells in visible and near-infrared channels. *J. Mater. Chem. B* **2017**, *5* (48), 9579−9590.
(54) Chen, T. H.; Zhang, S. W.; Jaishi, M.; Adhikari, R.; Bi, J. H.; Fang, M. X.; Xia, S.; Zhang, Y. B.; Luck, R. L.; Pati, R.; Lee, H. M.; Luo, F. T.; Tiwari, A.; Liu, H. Y. New Near-Infrared Fluorescent Probes with Single-Photon Anti-Stokes-Shift Fluorescence for Sensitive Determination of pH Variances in Lysosomes with a Double-Checked Capability. *ACS Appl. Bio Mater.* **2018**, *1* (3), 549−560.
(55) Wang, J. B.; Xia, S.; Bi, J. H.; Fang, M. X.; Mazi, W. F.; Zhang, Y. B.; Conner, N.; Luo, F. T.; Lu, H. P.; Liu, H. Y. Ratiometric Near-Infrared Fluorescent Probes Based On Through Bond Energy Transfer and pi-Conjugation Modulation between Tetraphenylethene and Hemicyanine Moieties for Sensitive Detection of pH Changes in Live Cells. *Bioconjugate Chem.* **2018**, *29* (4), 1406−1418.
(56) Xia, S.; Wang, J. B.; Bi, J. H.; Wang, X.; Fang, M. X.; Phillips, T.; May, A.; Conner, N.; Tanasova, M.; Luo, F. T.; Liu, H. Y. Fluorescent probes based on pi-conjugation modulation between hemicyanine and coumarin moieties for ratiometric detection of pH changes in live cells with visible and near-infrared channels. *Sensors and Actuators B-Chemical* **2018**, *265*, 699−708.
(57) Mazi, W.; Adhikari, R.; Zhang, Y. B.; Xia, S.; Fang, M. X.; Luck, R. L.; Tajiri, M.; Tiwari, A.; Tanasova, M.; Liu, H. Y. Fluorescent probes with high pKa values based on traditional, near-infrared rhodamine, and hemicyanine fluorophores for sensitive detection of lysosomal pH variations. *Methods* **2019**, *168*, 40−50.
(58) Zhang, Y. B.; Xia, S.; Mikesell, L.; Whisman, N.; Fang, M. X.; Steenwinkel, T. E.; Chen, K.; Luck, R. L.; Werner, T.; Liu, H. Y. Near-Infrared Hybrid Rhodol Dyes with Spiropyran Switches for Sensitive Ratiometric Sensing of pH Changes in Mitochondria and Drosophila melanogaster First-Instar Larvae. *ACS Appl. Bio Mater.* **2019**, *2* (11), 4986−4997.
(59) Mazi, W.; Yan, Y. N.; Zhang, Y. B.; Xia, S.; Wan, S. L.; Tajiri, M.; Luck, R. L.; Liu, H. Y. A near-infrared fluorescent probe based on a hemicyanine dye with an oxazolidine switch for mitochondrial pH detection. *J. Mater. Chem. B* **2021**, *9* (3), 857−863.
(60) Yan, Y. N.; Zhang, Y. B.; Xia, S.; Wan, S. L.; Vohs, T.; Tanasova, M.; Luck, R. L.; Liu, H. Y. Ratiometric Near-Infrared Fluorescent Probes Based on Hemicyanine Dyes Bearing Dithioacetal and Formal Residues for pH Detection in Mitochondria. *Molecules* **2021**, *26* (7), 2088.
(61) Frisch, M. J.; Trucks, G. W.; Schlegel, H. B.; Scuseria, G. E.; Robb, M. A.; Cheeseman, J. R.; Scalmani, G.; Barone, V.; Petersson, G. A.; Nakatsuji, H.; Li, X.; Caricato, M.; Marenich, A. V.; Bloino, J.; Janesko, B. G.; Gomperts, R.; Mennucci, B.; Hratchian, H. P.; Ortiz, J. V.; Izmaylov, A. F.; Sonnenberg, J. L.; Williams-Young, D.; Ding, F.; Lipparini, F.; Egidi, F.; Goings, J.; Peng, B.; Petrone, A.; Henderson, T.; Ranasinghe, D.; Zakrzewski, V. G.; Gao, J.; Rega, N.; Zheng, G.; Liang, W.; Hada, M.; Ehara, M.; Toyota, K.; Fukuda, R.; Hasegawa, J.; Ishida, M.; Nakajima, T.; Honda, Y.; Kitao, O.; Nakai, H.; Vreven, T.; Throssell, K.; Montgomery, J. A., Jr; Peralta, J. E.; Ogliaro, F.; Bearpark, M. J.; Heyd, J. J.; Brothers, E. N.; Kudin, K. N.; Staroverov, V. N.; Keith, T. A.; Kobayashi, R.; Normand, J.; Raghavachari, K.; Rendell, A. P.; Burant, J. C.; Iyengar, S. S.; Tomasi, J.; Cossi, M.; Millam, J. M.; Klene, M.; Adamo, C.; Cammi, R.; Ochterski, J. W.; Martin, R. L.; Morokuma, K.; Farkas, O.; Foresman, J. B.; Fox, D. J. *Gaussian 16, Revision A.03*; Gaussian, Inc.: Wallingford CT, 2016.
(62) Casida, M. E.; Jamorski, C.; Casida, K. C.; Salahub, D. R. Molecular excitation energies to high-lying bound states from time-dependent density-functional response theory: Characterization and correction of the time-dependent local density approximation ionization threshold. *J. Chem. Phys.* **1998**, *108*, 4439−4449.
(63) Cancès, E.; Mennucci, B.; Tomasi, J. A new integral equation formalism for the polarizable continuum model: Theoretical background and applications to isotropic and anistropic dielectrics. *J. Chem. Phys.* **1997**, *107*, 3032−3041.
(64) Dennington, R.; Keith, T. A.; Millam, J. M. *GaussView; 6, V.*; Semichem Inc.: Shawnee Mission, KS, 2016.
(65) Miyaura, N.; Suzuki, A. Palladium-Catalyzed Cross-Coupling Reactions of Organoboron Compounds. *Chem. Rev.* **1995**, *95*, 2457−2483.
(66) Adamo, C.; Barone, V. Toward reliable density functional methods without adjustable parameters: The PBE0 model. *J. Chem. Phys.* **1999**, *110* (13), 6158−6170.
(67) Yanai, T.; Tew, D.; Handy, N. A new hybrid exchange-correlation functional using the Coulomb-Attenuating Method (CAM-B3LYP). *Chem. Phys. Lett.* **2004**, *393*, 51−57.
(68) Lian, P.; Johnston, R. C.; Parks, J. M.; Smith, J. C. Quantum Chemical Calculation of pKas of Environmentally Relevant Functional Groups: Carboxylic Acids, Amines, and Thiols in Aqueous Solution. *J. Phys. Chem. A* **2018**, *122* (17), 4366−4374.
(69) Austin, A.; Petersson, G. A.; Frisch, M. J.; Dobek, F. J.; Scalmani, G.; Throssell, K. A Density Functional with Spherical Atom Dispersion Terms. *J. Chem. Theory Comput.* **2012**, *8* (12), 4989−5007.
(70) Tomasi, J.; Mennucci, B.; Cammi, R. Quantum Mechanical Continuum Solvation Models. *Chem. Rev.* **2005**, *105* (8), 2999−3094.
(71) Foresman, J. B.; Frisch, A. *Exploring Chemistry with Electronic Structure Methods*, 3rd ed.; Gaussian, Inc.: Wallingford, CT USA, 2015; p 531.
(72) Liptak, M. D.; Gross, K. C.; Seybold, P. G.; Feldgus, S.; Shields, G. C. Absolute pKa Determinations for Substituted Phenols. *J. Am. Chem. Soc.* **2002**, *124* (22), 6421−6427.
(73) Zielonka, J.; Joseph, J.; Sikora, A.; Hardy, M.; Ouari, O.; Vasquez-Vivar, J.; Cheng, G.; Lopez, M.; Kalyanaraman, B. Mitochondria-Targeted Triphenylphosphonium-Based Compounds: Syntheses, Mechanisms of Action, and Therapeutic and Diagnostic Applications. *Chem. Rev.* **2017**, *117* (15), 10043−10120.
(74) Reimer, R. J. Vesicular Neurotransmitter Transporters. In *Encyclopedia of Neuroscience*, Squire, L. R., Ed.; Academic Press: Oxford, 2009; pp 107−113.
(75) Giorgio, M.; Trinei, M.; Migliaccio, E.; Pelicci, P. G. Hydrogen peroxide: a metabolic by-product or a common mediator of ageing signals? *Nat. Rev. Mol. Cell Biol.* **2007**, *8* (9), 722−728.
(76) Wu, M. Y.; Li, K.; Liu, Y. H.; Yu, K. K.; Xie, Y. M.; Zhou, X. D.; Yu, X. Q. Mitochondria-targeted ratiometric fluorescent probe for real time monitoring of pH in living cells. *Biomaterials* **2015**, *53*, 669−678.
(77) Sun, J. Y.; Ling, P. H.; Gao, F. A Mitochondria-Targeted Ratiometric Biosensor for pH Monitoring and Imaging in Living Cells with Congo-Red-Functionalized Dual-Emission Semiconducting Polymer Dots. *Anal. Chem.* **2017**, *89* (21), 11703−11710.
(78) Xue, F. F.; Du, W. X.; Chen, S. X.; Ma, M.; Kuang, Y. C.; Chen, J. F.; Yi, T.; Chen, H. R. Hypoxia-Induced Photogenic Radicals by Eosin Y for Efficient Phototherapy of Hypoxic Tumors. *ACS Appl. Bio Mater.* **2020**, *3* (12), 8962−8969.
(79) Wan, S. L.; Vohs, T.; Steenwinkel, T. E.; White, W. R.; Lara-Ramirez, A.; Luck, R. L.; Werner, T.; Tanasova, M.; Liu, H. Y. Near-Infrared Fluorescent Probes with Amine-Incorporated Xanthene Platforms for the Detection of Hypoxia. *ACS Appl. Bio Mater.* **2022**, *5* (9), 4294−4300.
(80) Yoon, S. A.; Chun, J.; Kang, C.; Lee, M. H. Self-Calibrating Bipartite Fluorescent Sensor for Nitroreductase Activity and Its Application to Cancer and Hypoxic Cells. *Acs Applied Bio Materials* **2021**, *4* (3), 2052−2057.

https://doi.org/10.1021/acsomega.4c07303
ACS Omega 2024, 9, 42049−42060